LETTER

doi:10.1038/nature23289

Significant and variable linear polarization during the prompt optical flash of GRB 160625B

E. Troja[1,2], V. M. Lipunov[3,4], C. G. Mundell[5], N. R. Butler[6], A. M. Watson[7], S. Kobayashi[8], S. B. Cenko[1,2], F. E. Marshall[2], R. Ricci[9], A. Fruchter[10], M. H. Wieringa[11], E. S. Gorbovskoy[3,4], V. Kornilov[3,4], A. Kutyrev[1,2], W. H. Lee[7], V. Toy[1], N. V. Tyurina[3,4], N. M. Budnev[12], D. A. H. Buckley[13], J. González[7], O. Gress[12], A. Horesh[14], M. I. Panasyuk[15], J. X. Prochaska[16], E. Ramirez-Ruiz[16], R. Rebolo Lopez[17], M. G. Richer[18], C. Román-Zúñiga[18], M. Serra-Ricart[17], V. Yurkov[19] & N. Gehrels[2]

Newly formed black holes of stellar mass launch collimated outflows (jets) of ionized matter that approach the speed of light. These outflows power prompt, brief and intense flashes of γ-rays known as γ-ray bursts (GRBs), followed by longer-lived afterglow radiation that is detected across the electromagnetic spectrum. Measuring the polarization of the observed GRB radiation provides a direct probe of the magnetic fields in the collimated jets. Rapid-response polarimetric observations of newly discovered bursts have probed the initial afterglow phase[1–3], and show that, minutes after the prompt emission has ended, the degree of linear polarization can be as high as 30 per cent—consistent with the idea that a stable, globally ordered magnetic field permeates the jet at large distances from the central source[3]. By contrast, optical[4–6] and γ-ray[7–9] observations during the prompt phase have led to discordant and often controversial[10–12] results, and no definitive conclusions have been reached regarding the origin of the prompt radiation or the configuration of the magnetic field. Here we report the detection of substantial (8.3 ± 0.8 per cent from our most conservative simulation), variable linear polarization of a prompt optical flash that accompanied the extremely energetic and long-lived prompt γ-ray emission from GRB 160625B. Our measurements probe the structure of the magnetic field at an early stage of the jet, closer to its central black hole, and show that the prompt phase is produced via fast-cooling synchrotron radiation in a large-scale magnetic field that is advected from the black hole and distorted by dissipation processes within the jet.

On 25 June 2016 at 22:40:16.28 Universal Time (UT), the γ-ray burst monitor (GBM) aboard NASA's Fermi Gamma-ray Space Telescope discovered GRB 160625B as a short-lived pulse (lasting about 1 second) of γ-ray radiation (G1 in Fig. 1). An automatic localization was published rapidly by the spacecraft, allowing wide-field optical facilities to start follow-up observations. Three minutes after the first alert, at 22:43:24.82 UT (hereafter T_0), the Large Area Telescope (LAT) aboard Fermi was triggered by another bright but longer-lasting pulse (of about 30 seconds; G2 in Fig. 1), visible up to gigaelectronvolt (GeV) energies[13]. A rapid increase in brightness was observed simultaneously at optical wavelengths (Fig. 1): the optical brightness rose by a factor of 100 in a few seconds, reaching its peak at $T_0 + 5.9$ seconds, with an observed visual magnitude of 7.9. After a second, fainter peak at $T_0 + 15.9$ seconds, the optical light declined steadily. During this phase, the MASTER[14]-IAC telescope on Tenerife, Spain, observed the optical counterpart in two orthogonal polaroids simultaneously, starting at $T_0 + 95$ seconds and ending at $T_0 + 360$ seconds. The detection of a polarized signal with this instrumental configuration provides a lower bound ($\Pi_{\rm L,min}$) to the true degree of linear polarization, thus $\Pi_{\rm L,min} = (I_2 - I_1)/(I_1 + I_2)$, where I_1 and I_2 refer to the source intensity in each polaroid. Substantial levels of linear polarization, up to $\Pi_{\rm L,min} = 8.0 \pm 0.5\%$, were thereby detected (Fig. 2; by comparison, values of less than 2% have been detected for other nearby objects of similar brightness). Over this time interval a weak tail of γ-ray emission was visible, until the onset of a third, longer-lived episode of

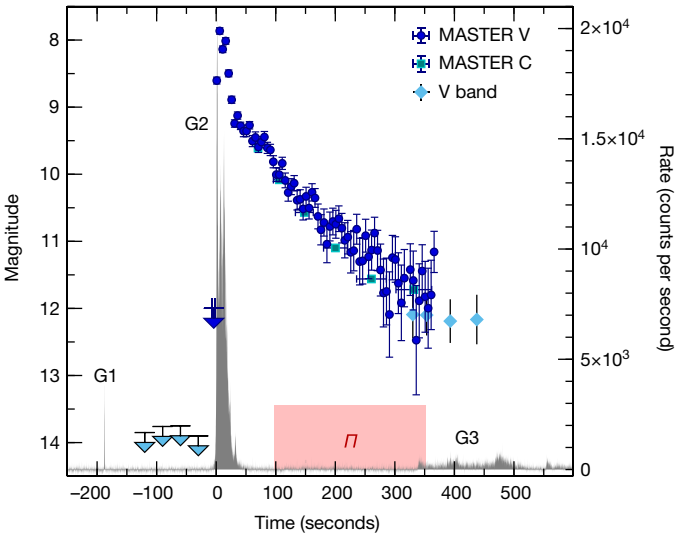

Figure 1 | Prompt γ-ray and optical light curves of GRB 160625B. The γ-ray light curve (black; 10–250 keV) consists of three main episodes: a short precursor (G1), a bright main burst (G2), and a fainter and longer-lasting tail (G3). Optical data from the MASTER Net telescopes and other ground-based facilities[19] are overlaid for comparison. Error bars represent 1σ; upper limits are 3σ. The red box marks the time interval over which polarimetric measurements were taken. Within the sample of nearly 2,000 bursts detected by the GBM, only six other events have a comparable duration (https://heasarc.gsfc.nasa.gov/W3Browse/fermi/fermigbrst.html). Most GRBs end before the start of polarimetric observations.

[1]Department of Astronomy, University of Maryland, College Park, Maryland 20742-4111, USA. [2]NASA Goddard Space Flight Center, 8800 Greenbelt Rd, Greenbelt, Maryland 20771, USA. [3]M.V. Lomonosov Moscow State University, Physics Department, Leninskie Gory, GSP-1, Moscow 119991, Russia. [4]M.V. Lomonosov Moscow State University, Sternberg Astronomical Institute, Universitetsky Prospekt, 13, Moscow 119234, Russia. [5]Department of Physics, University of Bath, Claverton Down, Bath BA2 7AY, UK. [6]School of Earth and Space Exploration, Arizona State University, Tempe, Arizona 85287, USA. [7]Instituto de Astronomía, Universidad Nacional Autónoma de México, Apartado Postal 70-264, 04510 Ciudad de México, México. [8]Astrophysics Research Institute, Liverpool John Moores University, IC2 Building, Liverpool Science Park, 146 Brownlow Hill, Liverpool L3 5RF, UK. [9]INAF-Istituto di Radioastronomia, Via Gobetti 101, I-40129 Bologna, Italy. [10]Space Telescope Science Institute, 3700 San Martin Drive, Baltimore, Maryland 21218, USA. [11]CSIRO Astronomy and Space Science, PO Box 76, Epping, New South Wales 1710, Australia. [12]Irkutsk State University, Applied Physics Institute, 20 Gagarin Boulevard, 664003 Irkutsk, Russia. [13]South African Astronomical Observatory, PO Box 9, 7935 Observatory, Cape Town, South Africa. [14]Racah Institute of Physics, Hebrew University, Jerusalem 91904, Israel. [15]Skobeltsyn Institute of Nuclear Physics of Lomonosov, Moscow State University, Vorob'evy Gory, 119991 Moscow, Russia. [16]University of California Observatories, 1156 High Street, Santa Cruz, California 95064, USA. [17]Instituto de Astrofísica de Canarias Via Lactea, s/n E38205, La Laguna, Tenerife, Spain. [18]Instituto de Astronomía, Universidad Nacional Autónoma de México, Apartado Postal 106, 22800 Ensenada, Baja California, México. [19]Blagoveshchensk State Pedagogical University, Lenin Street 104, Amur Region, Blagoveshchensk 675000, Russia.

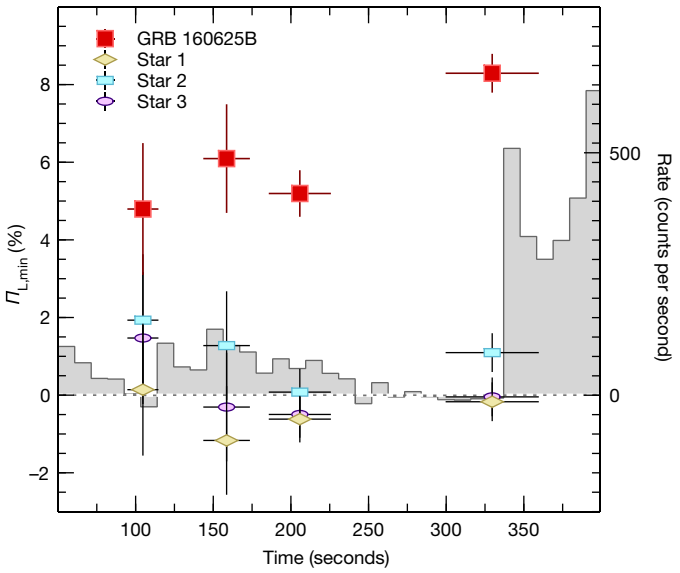

Figure 2 | Temporal evolution of the optical polarization measured for GRB 160625B. The minimum polarization ($\Pi_{L,min}$), measured in four different temporal bins (red squares), remains fairly constant over the first three exposures, then increases by 60% during the fourth (and last) observation. At the same time, an evident increase in the γ-ray count rates (grey shaded area; 5-second time bins) marks the onset of the third episode of prompt emission (G3 in Fig. 1). The spectral shape and fast temporal variability observed during G3 are typical of a GRB's prompt emission. For comparison, we also show simultaneous polarimetric measurements of the three brightest stars in the MASTER-IAC field of view. Error bars represent 1σ.

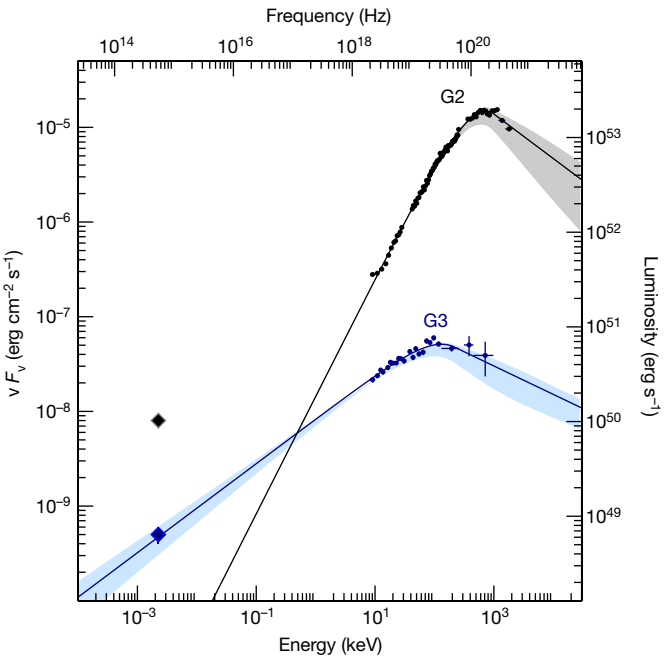

Figure 3 | Broadband spectra of the prompt phase in GRB 160625B. Spectra are shown for the two main episodes of prompt emission, G2 and G3. Error bars represent 1σ. The γ-ray spectra were modelled with a smoothly broken power law (solid lines). The 1σ uncertainty in the best-fit model is shown by the shaded area. The diamonds indicate the average optical flux (corrected for galactic extinction) observed during the same time intervals. The extrapolated contribution of the prompt γ-ray component to the optical band is non-negligible during episode G3, and constitutes more than 40% of the observed emission.

prompt γ-ray radiation (G3), starting at T_0+337 seconds and ending at T_0+630 seconds.

In the standard GRB model[15,16], after a jet is launched, dissipation processes within the ultra-relativistic flow produce a prompt flash of radiation, mostly visible as γ-rays. Later, the jet's outermost layers interact with the surrounding medium and two shocks develop, one propagating outwards into the external medium (the forward shock) and the other one travelling backwards into the jet (the reverse shock). These shocks heat up the ambient electrons, which emit, via synchrotron emission, a broadband afterglow radiation. At an early time (around T_0+10 seconds), the observed optical flux from GRB 160625B is orders of magnitude brighter than the extrapolated prompt emission component (Fig. 3), suggesting that optical and γ-ray emissions originate from different physical locations in the flow. A plausible interpretation is that the early (around T_0+10 seconds) optical emission arises from a strong reverse shock, although internal dissipation processes are also possible (see Methods).

A general prediction of the reverse-shock model[17] is that, after reaching its peak, the optical flash should decay as a smooth power law with slope of -2. However, in our case, the optical light curve is more complex: its temporal decay is described by a series of power-law segments with slopes of between -0.3 and -1.8. The shallower decay could be explained in part by the ejection of a range of Lorentz factors, as the blastwave is refreshed by the arrival of the more slowly moving ejecta[18]. But this would require *ad hoc* choices of the Lorentz-factor distribution in order to explain each different power-law segment, and does not account for the observed temporal evolution of the polarization. Our observations are more naturally explained by including a second component of emission in the optical range, a component that dominates at times later than T_0+300 seconds. Our broadband spectral analysis (see Methods) rules out a large contribution from the forward shock, whose emission is negligible at this time (less than 1 mJy). Instead, the prompt optical component makes a substantial contribution (more than 40%) to the observed optical light (Fig. 3).

The only other known time-resolved polarimetric study[3] showed that the properties of the reverse shock remain roughly constant over time. Our measurements hint at a different temporal trend. The fractional polarization seems to be stable over the first three exposures, and changes with high significance (about 99.9996%) in the last temporal bin (Fig. 2). On the basis of our broadband dataset, we can confidently rule out geometric effects as the cause of the observed change: if the observer's line of sight were to intercept the jet edges, then a steeper decay of the optical flux would be seen, and this would not also be consistent with the achromatic jet-break detected at much later times (Extended Data Fig. 1). The temporal correlation between the γ-ray flux and the fractional polarization (Fig. 2), as well as the substantial contribution of the prompt component to the optical emission (Fig. 3), suggests that the γ-ray and optical photons are located together, and that the observed variation in $\Pi_{L,min}$ is connected to the renewed jet activity. Thus our last observation detected the linear optical polarization of the prompt emission, directly probing the jet properties at the smaller radius from which prompt optical and γ-ray emissions originate.

Three main emission mechanisms are commonly invoked to explain the prompt GRB phase, and all three of them can in principle lead to a substantial level of polarization. However, inverse Compton scattering and photospheric emission could lead to non-zero polarization only if the spherical symmetry of the emitting patch were broken by the jet edges. But, as explained above, an off-axis model is not consistent with our dataset. Furthermore, an inverse Compton origin of the observed prompt phase would imply a prominent high-energy (above 1 GeV) component, in contrast with observations[19]. The most plausible source of the observed photons is synchrotron radiation from a population of fast-cooling electrons moving in strong magnetic fields. This could account for the low-energy spectral slope α (about -1.5; see Methods) and the high degree of polarization. An analogous conclusion, based on different observational evidence, was reached by an independent study of this burst[19].

If the magnetic field were to be produced by local instabilities in the shock front, then the polarized radiation would come from several

independent patches with different field orientations. This model does not fit our data well. It predicts erratic fluctuations of the polarization angle, and a maximum level of polarization[20,21] of $\Pi_{\max} \approx \Pi_{\rm syn}/\sqrt{N} \approx$ 2–3%, where the intrinsic polarization of the synchrotron radiation, $\Pi_{\rm syn}$, is about 70% (ref. 22), and the number of magnetic patches, N, is about 1,000 (ref. 23). Our observations are instead easily accommodated if there is a large-scale magnetic field advected from the central source. Recent claims of a variable polarization angle during the prompt γ-ray emission hinted, although not unambiguously, at a similar configuration[9].

This model[21,24] can explain the stable polarization measurements, the high degree of polarization, and the rapid change in polarization when the new prompt episode begins. In this model, the magnetic field is predominantly toroidal, and the polarization angle is constant. If relativistic aberration is taken into account[24], then the polarization degree can be as high as some 50%. In this case, the probability of measuring a polarization as low as $\Pi_{\rm L,min} \approx 8\%$ is approximately 10% (see Methods). It seems more likely that the actual polarization degree is lower than the maximum possible value and closer to our measurement, suggesting that the large-scale magnetic field might be substantially distorted by internal collisions[25,26] or by kink instabilities[27] at smaller radii before the reconnection process produces bright γ-rays.

Our results suggest that GRB outflows might be launched as jets dominated by Poynting flux, whose magnetic energy is dissipated rapidly close to the source, after which they propagate as hot baryonic jets with a relic magnetic field. A large-scale magnetic field is therefore a generic property of GRB jets, and the production of a bright optical flash depends on how jet instabilities develop near the source and how efficiently these instabilities suppress magnetic fields. The dissipation of the primordial magnetic field at the internal radius, as observed for GRB 160625B, is essential for the efficient acceleration of particles to the highest energies (of more than 10^{20} eV)[25,28]. However, the ordered superluminal component at the origin of the observed polarization and the relatively high magnetization (about 0.1; see Methods) of the ejecta might hinder the acceleration of particles by shocks[28], thus suggesting either that GRBs are not bright sources of ultrahigh-energy cosmic rays as previously thought, or that other acceleration mechanisms[29] need to be considered.

Online Content Methods, along with any additional Extended Data display items and Source Data, are available in the online version of the paper; references unique to these sections appear only in the online paper.

Received 21 February; accepted 7 June 2017.

1. Mundell, C. G. *et al.* Early optical polarization of a gamma-ray burst afterglow. *Science* **315,** 1822–1824 (2007).
2. Steele, I. A., Mundell, C. G., Smith, R. J., Kobayashi, S. & Guidorzi, C. Ten per cent polarized optical emission from GRB090102. *Nature* **462,** 767–769 (2009).
3. Mundell, C. G. *et al.* Highly polarized light from stable ordered magnetic fields in GRB 120308A. *Nature* **504,** 119–121 (2013).
4. Kopač, D. *et al.* Limits on optical polarization during the prompt phase of GRB 140430A. *Astrophys. J.* **813,** 1 (2015).
5. Pruzhinskaya, M. V. *et al.* Optical polarization observations with the MASTER robotic net. *New Astron.* **29,** 65–74 (2014).
6. Gorbovskoy, E. S. *et al.* Early polarization observations of the optical emission of gamma-ray bursts: GRB 150301B and GRB 150413A. *Mon. Not. R. Astron. Soc.* **455,** 3312–3318 (2016).
7. Coburn, W. & Boggs, S. E. Polarization of the prompt γ-ray emission from the γ-ray burst of 6 December 2002. *Nature* **423,** 415–417 (2003).
8. Götz, D., Laurent, P., Lebrun, F., Daigne, F. & Bošnjak, Ž. Variable polarization measured in the prompt emission of GRB 041219A using IBIS on board INTEGRAL. *Astrophys. J.* **695,** L208–L212 (2009).
9. Yonetoku, D. *et al.* Magnetic structures in gamma-ray burst jets probed by gamma-ray polarization. *Astrophys. J.* **758,** L1 (2012).
10. Rutledge, R. E. & Fox, D. B. Re-analysis of polarization in the γ-ray flux of GRB 021206. *Mon. Not. R. Astron. Soc.* **350,** 1288–1300 (2004).
11. McGlynn, S. *et al.* Polarization studies of the prompt gamma-ray emission from GRB 041219a using the spectrometer aboard INTEGRAL. *Astron. Astrophys.* **466,** 895–904 (2007).
12. Kalemci, E., Boggs, S. E., Kouveliotou, C., Finger, M. & Baring, M. G. Search for polarization from the prompt gamma-ray emission of GRB 041219a with SPI on INTEGRAL. *Astrophys. J.* **169** (Supp.), 75–82 (2007).
13. Dirirsa, F., Racusin, J., McEnery, J. & Desiante, R. GRB 160625B: Fermi-LAT detection of a bright burst. *GCN Circ.* **19580,** https://gcn.gsfc.nasa.gov/other/160625B.gcn3 (2016)
14. Lipunov, V. *et al.* Master robotic net. *Adv. Astron.* **2010,** 349171 (2010).
15. Piran, T. Gamma-ray bursts and the fireball model. *Phys. Rep.* **314,** 575–667 (1999).
16. Kumar, P. & Zhang, B. The physics of gamma-ray bursts relativistic jets. *Phys. Rep.* **561,** 1–109 (2015).
17. Kobayashi, S. Light curves of gamma-ray burst optical flashes. *Astrophys. J.* **545,** 807–812 (2000).
18. Sari, R. & Mészáros, P. Impulsive and varying injection in gamma-ray burst afterglows. *Astrophys. J.* **535,** L33–L37 (2000).
19. Zhang, B.-B. *et al.* Transition from fireball to Poynting-flux-dominated outflow in three-episode GRB 160625B. Preprint at https://arxiv.org/abs/1612.03089 (2016)
20. Gruzinov, A. & Waxman, E. Gamma-ray burst afterglow: polarization and analytic light curves. *Astrophys. J.* **511,** 852–861 (1999).
21. Granot, J. & Königl, A. Linear polarization in gamma-ray bursts: the case for an ordered magnetic field. *Astrophys. J.* **594,** L83–L87 (2003).
22. Rybicki, G. B. & Lightman, A. P. *Radiative Processes in Astrophysics* (Wiley-Interscience, 1979).
23. Inoue, T., Asano, K. & Ioka, K. Three-dimensional simulations of magnetohydrodynamic turbulence behind relativistic shock waves and their implications for gamma-ray bursts. *Astrophys. J.* **734,** 77 (2011).
24. Lyutikov, M., Pariev, V. I. & Blandford, R. D. Polarization of prompt gamma-ray burst emission: evidence for electromagnetically dominated outflow. *Astrophys. J.* **597,** 998–1009 (2003).
25. Zhang, B. & Yan, H. The internal-collision-induced magnetic reconnection and turbulence (ICMART) model of gamma-ray bursts. *Astrophys. J.* **726,** 90 (2011).
26. Deng, W., Zhang, H., Zhang, B. & Li, H. Collision-induced magnetic reconnection and a unified interpretation of polarization properties of GRBs and blazars. *Astrophys. J.* **821,** L12 (2016).
27. Bromberg, O. & Tchekhovskoy, A. Relativistic MHD simulations of core-collapse GRB jets: 3D instabilities and magnetic dissipation. *Mon. Not. R. Astron. Soc.* **456,** 1739–1760 (2016).
28. Sironi, L. & Spitkovsky, A. Particle acceleration in relativistic magnetized collision-less electron-ion shocks. *Astrophys. J.* **726,** 75 (2011).
29. Giannios, D. UHECRs from magnetic reconnection in relativistic jets. *Mon. Not. R. Astron. Soc.* **408,** L46–L50 (2010).

Acknowledgements E.T. thanks L. Piro and K. Murase for comments. We thank the RATIR (Reionization And Transients InfraRed) project team and the staff of the Observatorio Astronómico Nacional on Sierra San Pedro Mártir, and acknowledge the contribution of L. Georgiev and J.S. Bloom to the development of this observatory. RATIR is a collaboration between the University of California, the Universidad Nacional Autonóma de México, the NASA Goddard Space Flight Center and Arizona State University, and benefits from the loan of an H2RG detector and hardware and software support from Teledyne Scientific and Imaging. RATIR, the automation of the Harold L. Johnson Telescope of the Observatorio Astronómico Nacional on Sierra San Pedro Mártir, and the operation of both are funded through NASA grants NNX09AH71G, NNX09AT02G, NNX10AI27G and NNX12AE66G, CONACyT grants INFR-2009-01-122785 and CB-2008-101958, UNAM PAPIIT grant IN113810, and UC MEXUS-CONACyT grant CN 09-283. The MASTER project is supported in part by the Development Program of Lomonosov Moscow State University, Moscow Union OPTICA, Russian Science Foundation grant 16-12-00085. This work was supported in part by NASA Fermi grants NNH14ZDA001N and NNH15ZDA001N. This work made use of data supplied by the UK Swift Science Data Centre at the University of Leicester, funded by the UK Space Agency.

Author Contributions E.T., C.G.M. and S.K. composed the text on the basis of inputs from all authors. MASTER data were provided, reduced and analysed by V.M.L., E.S.G. and N.V.T. RATIR observations were obtained, reduced and analysed by N.R.B., E.T., A.M.W., A.K., W.H.L. and V.T. F.E.M. processed and analysed the Swift/Ultraviolet–Optical Telescope (UVOT) data. E.T., R.R. and M.H.W. obtained, processed and analysed the Australian Telescope Compact Array (ATCA) observations (E.T. was the principal investigator). Jansky Very Large Array (VLA) observations were obtained, processed and analysed by S.B.C., A.F. and A.H. (with S.B.C. being the principal investigator). All authors helped to obtain parts of the presented dataset, to discuss the results or to comment on the manuscript.

Author Information Reprints and permissions information is available at www.nature.com/reprints. The authors declare no competing financial interests. Readers are welcome to comment on the online version of the paper. Publisher's note: Springer Nature remains neutral with regard to jurisdictional claims in published maps and institutional affiliations. Correspondence and requests for materials should be addressed to E.T. (eleonora.troja@nasa.gov).

Reviewer Information *Nature* thanks D. Giannios and the other anonymous reviewer(s) for their contribution to the peer review of this work.

METHODS

MASTER observations. The MASTER-IAC telescope, located at Teide Observatory (Tenerife, Spain), responded to the first GBM alert and started observing the field with its very-wide-field camera at T_0-133 seconds. Observations were made with a constant integration time of 5 seconds and ended at T_0+350 seconds. The MASTER II telescope responded to the LAT alert[13] and observed the GRB position between T_0+65 seconds and T_0+360 seconds. The resulting light curves are shown in Fig. 1. Polarimetric observations started at T_0+95 seconds in response to the LAT trigger. However, owing to a software glitch, these observations were scheduled as a series of tiled exposures covering a larger area. This caused the telescope to slew away from the true position of the burst at T_0+360 seconds. A total of four useful exposures was collected (Extended Data Table 1). Data were reduced in a standard fashion[5,14]. The two synchronous frames used to measure the polarization were mutually calibrated so that the average polarization for comparison stars is zero; this procedure removes the effects of interstellar polarization. The significance of the polarimetric measurements was assessed through Monte Carlo simulations. Extended Data Fig. 2 shows the resulting distribution of polarization values and significances.

Observations by the Swift spacecraft. Observations by the GRB explorer Swift span the period from $T_0+9.6$ ks to T_0+48 days. Swift X-ray telescope (XRT) data were collected in photon-counting mode for a total net exposure of 134 ks. The optical afterglow was monitored with the UVOT in the *u*, *v*, and *w1* filters for ten days after the burst, after which it fell below the detection threshold of the UVOT. Subsequent observations were performed using the UVOT filter of the day. Swift data were processed using Swift software within the HEASOFT v6.19 software package. We used the latest release of the XRT and UVOT calibration database and followed standard data-reduction procedures. Aperture photometry on the UVOT images was performed using a circular region of radius 2.5″ centred on the afterglow position. When necessary, adjacent exposures were co-added in order to increase the signal. We adopted the standard photometric zero points in the Swift UVOT calibration database[30]. The resulting Swift light curves are shown in Extended Data Fig. 1.

RATIR observations. RATIR obtained simultaneous multicolour (riZYJH) imaging of GRB 160625B, starting at T_0+8 hours, and monitored the afterglow for the following 50 days until it fell below its detection threshold. RATIR data were reduced and analysed using standard astronomy algorithms. Aperture photometry was performed with SExtractor[31], and the resulting instrumental magnitudes were compared to Pan-STARRS1 in the optical filters[32] and 2MASS in the near-infrared filters[33] to derive the image zero points. Our final optical and infrared photometry is shown in Extended Data Fig. 1.

Radio observations. Radio observations were carried out with the ATCA and VLA. The ATCA radio observations were carried out on 30 June 2016 ($T_0+4.5$ days) at the centre frequencies of 5.5 GHz, 7.5 GHz, 38 GHz and 40 GHz; on 11 July 2016 ($T_0+15.7$ days) at the centre frequencies of 18 GHz, 20 GHz, 38 GHz and 40 GHz; and on 24 July 2016 ($T_0+28.6$ days) at the centre frequencies of 8 GHz, 10 GHz, 18 GHz and 20 GHz. For all epochs, the frequency bandwidth was 2 GHz and the array configuration was H75. A standard calibrator (the radio source PKS 1934-638) was observed to obtain the absolute flux-density scale. The phase calibrators were PKS 2022+031 for observations at 5.5–10 GHz, and PKS 2059+034 for observations at 18–40 GHz. The data were flagged, calibrated and imaged with standard procedures in the data-reduction package MIRIAD[34]. Multifrequency synthesis images were formed at 6.5 GHz, 7.5 GHz, 9 GHz, 19 GHz and 39 GHz. The target appeared point-like in all restored images.

The VLA observed the afterglow in three different epochs: 30 June 2016, 9 July 2016, and 27 July 2016. For all of our observations, we used the γ-ray blazar J2049+1003 as the phase calibrator, and the active galactic nucleus 3C48 as the flux calibrator. The observations were undertaken at central frequencies of 6 GHz (C-band) and 22 GHz (K-band), with bandwidths of 4 GHz and 8 GHz, respectively. The data were calibrated using standard tools in the CASA software and then imaged with the clean task. The source was significantly (more than 5σ) detected in all three observations and in all bands. The radio afterglow light curve at 10 GHz is shown in Extended Data Fig. 1.

Spectral properties of the prompt GRB phase. GRB 160625B is characterized by three distinct episodes of prompt γ-ray emission, separated by long periods of apparent quiescence (Fig. 1). A detailed spectral analysis of the first two episodes (G1 and G2) is presented elsewhere[19], and shows that the first event, G1, is well described by a thermal component with temperature (kT) values of about 1 keV, while the second episode, G2, is dominated by a non-thermal component that peaks at energies of less than around 500 keV and which is consistent with synchrotron emission in a decaying magnetic field[35]. Our spectral analysis focuses on the third event, G3.

We selected the time intervals for our analysis on the basis of the properties of the γ-ray and optical light curves. We retrieved GBM data from the public archive and inspected them using the standard RMFIT software tool. The variable γ-ray background in each energy channel was modelled by a series of polynomial functions. Spectra were binned in order to have at least one count per spectral bin, and were fit within the X-ray spectral fitting package XSPEC[36] by minimizing the modified Cash statistics (W-stat). We used a Band function[37] to model the spectra, and fixed the high-energy index to $\beta=-2.3$ when the data could not constrain it. The best-fit model was then extrapolated to lower energies in order to estimate the contribution of the prompt component at optical frequencies. During the main γ-ray episode (G2), the observed optical emission is several orders of magnitude brighter than the extrapolation of the prompt component. By contrast, we found that the later prompt phase (G3) contributes substantially to the observed optical flux. This is rare but not unprecedented[38–40]: it has been shown that most GRBs have an optical emission that is fainter than $R=15.5$ mag when the γ-ray emission is active; however, a small fraction (around 5–20%) exhibits a bright ($R\geq 14$ mag) optical counterpart during the prompt phase[41].

As a further test, we carried out a joint time-resolved analysis of the optical and γ-ray data during G3. The results are summarized in Extended Data Table 2. The derived broadband spectra are characterized by a low-energy photon index of –1.5, consistent with fast-cooling synchrotron radiation (where ν_c, the cooling frequency, is less than ν_m, the synchrotron frequency). Our analysis constrains the spectral peak at $\nu_m\approx 2\times10^{19}$ Hz and, for the conditions typical of internal dissipation models, the cooling frequency of the emitting electrons is $\nu_c\approx 5\times10^{12}\,(\varepsilon_B/0.1)^{-3/2}$ Hz $<<\nu_{opt}<<\nu_m$, wherein we adopted the standard assumption that the magnetic energy is a constant fraction, ε_B, of the internal energy generated in the prompt dissipation process. Given that the synchrotron self-absorption might suppress the emission at low frequencies, we consider below whether it affects the optical band. A simple estimate of the maximal flux is given by a blackbody emission with the electron temperature $k_BT\approx\gamma_e m_e c^2$, thus:

$$F_{\nu,\mathrm{BB}}=2\pi\nu^2(1+z)^3\Gamma\gamma_e m_e\left(\frac{R_\perp}{D_L}\right)^2$$

where the observed frequency, ν, is about 5.5×10^{14} Hz; the GRB's redshift, z, is 1.406; the electron's Lorentz factor is $\gamma_e\propto\nu^{1/2}$; Γ is the bulk Lorentz factor; the luminosity distance, D_L, is about 3×10^{28} cm; and the fireball size for the observer is $R_\perp$, which depends on the emission radius R_e as $R_\perp\sim R_e/\Gamma$. By imposing the condition that the blackbody limit is larger than the observed optical flux, F_ν, of about 90 mJy, we obtain a lower limit to the emission radius[39]:

$$R_{\min}\approx 4\times10^{14}\left(\frac{\Gamma}{200}\right)^{\frac{2}{5}}\left(\frac{\varepsilon_B}{0.1}\right)^{\frac{1}{10}}\left(\frac{E_{\gamma,\mathrm{iso}}}{10^{53}\mathrm{erg}}\right)^{\frac{1}{10}}\left(\frac{\Delta T}{300s}\right)^{\frac{-1}{10}}\ \mathrm{cm} \qquad (1)$$

where ΔT is the duration of the G3 burst, and $E_{\gamma,\mathrm{iso}}$ is the isotropic equivalent γ-ray energy released over ΔT. The radius derived in equation (1) is within the acceptable range for internal dissipation models, in particular those invoking the dissipation of large-scale magnetic fields[25,29] as suggested by our polarization measurements. For emission radii larger than $R_{\min}$, the synchrotron self-absorption does not affect the optical emission, in agreement with our observations of a single power-law segment from optical to hard X-rays. These results lend further support to our conclusions.

Origin of the early optical emission. One of the main features of GRB 160625B is its extremely bright optical emission during the prompt phase (Fig. 1). In the previous section we showed that, during G3, the data support a common origin for the optical and γ-ray photons, consistent with a standard fast-cooling synchrotron emission. Our analysis also showed that the same conclusion does not hold at earlier times. During the main burst (G2), the observed emission cannot be explained by a single spectral component (Fig. 3). Distinct physical origins for the optical and γ-ray emissions are also suggested by the time lag between their light curves (Extended Data Fig. 3).

A plausible interpretation is that the bright optical flash is powered by the reverse shock, and is unrelated to the prompt γ-ray emission during G2. In this framework, our first three polarization measurements probe the fireball ejecta at the larger reverse-shock radius, and only the fourth observation includes the major contribution of the prompt phase. This model can consistently explain the early optical and radio observations, as shown in more detail below. However, in its basic form[17], the reverse-shock emission cannot explain the rapid rise and double-peaked structure of the optical light curve.

A different possibility is that the early optical emission is produced by the same (or similar) mechanisms that power the prompt γ-ray phase, which would naturally explain the initial sharp increase in the observed flux, as well as its variability. One of the most popular hypotheses is that the optical and γ-ray photons are produced by two different radiation mechanisms[42]: synchrotron radiation for the optical photons, and synchrotron self-Compton (SSC) radiation for the γ-rays. This model faces several problems, however, in particular the lack of a temporal

correlation between the low- and high-energy light curves, and the absence of a bright second-order inverse Compton component. Another possibility is a two-component synchrotron radiation from internal shocks in a highly variable outflow[43]. This model predicts a weak high-energy emission and a delayed onset for the optical emission, consistent with the observations. However, it presents other limitations, such as an excessive energy budget and an unusually high variability of Lorentz factors.

In a different set of models, the optical and γ-ray photons come from two distinct emitting zones within the flow. For example, in the magnetic reconnection model[44], a bright quasi-thermal component—emitted at the photospheric radius—peaks in the hard X-rays, while standard synchrotron emission from larger radii is observed in the optical emission. This can explain most of the properties of the G2 episode, but it does not reproduce well the observed spectral shape: the low-energy spectral slope measured during this interval[19] is too shallow to be accounted for by the Rayleigh–Jeans tail of the thermal spectrum.

The properties of the G2 episode are best explained by models in which the optical and γ-ray photons arise from synchrotron radiation at different laboratory times[45] or in different emitting regions. These are, for example, late internal shocks from residual collisions[46] or the decay of free neutrons[47]. In this framework, the steep decay phase observed after the second optical peak could be powered by delayed prompt emission from higher latitudes with respect to the observer's line of sight. This case, in which all of the polarization measurements probe the prompt emission mechanisms, only strengthens our finding that the prompt optical emission is inherently polarized.

Polarization. Synchrotron radiation is inherently highly polarized. For a power-law energy distribution of the emitting electrons ($\mathrm{d}n/\mathrm{d}E \propto E^{-p}$) (where n is the number of electrons, E is their energy and p is their spectral index), the intrinsic linear polarization ($\Pi_{\rm syn}$) at low frequencies is 9/13 (or about 70%). If an ordered magnetic field permeates the GRB jet, then each emitting region generates the maximum polarization $\Pi_{\rm syn}$. However, owing to relativistic kinematic effects, the average polarization within the Γ^{-1} field of view is smaller and here we assume that $\Pi_{\rm max}$ is about 50% for the regime $\nu_{\rm c} < \nu < \nu_{\rm m}$.

Given that an observer can see only a small area around the line of sight, owing to the relativistic beaming, the magnetic field can be considered to be parallel within the visible area. Our measured value $\Pi_{\rm L,min}$ is related to the true degree of polarization as $\Pi_{\rm L,min} = \Pi_{\rm L} \cos 2\theta$, where θ is the angle between the polarization direction and the x-axis of the reference system. For a random orientation of the observer, if $\Pi_{\rm L} \approx \Pi_{\rm max}$, then the chance of detecting a polarization lower than an $\Pi_{\rm L,min}$ of about 8% is small (about 10%). The observed values of $\Pi_{\rm L,min}$ suggest that the magnetic field is largely distorted even on small angular scales of about $1/\Gamma$, but is not yet completely tangled.

As the detected optical light is a mixture of reverse shock and prompt emission, we now consider whether our polarization measurements require the magnetic field to be distorted in both of the emitting regions. In our last polarimetric observation, the prompt and reverse-shock components contribute roughly equally to the observed light, so that $\Pi_{\rm L,min} = (\Pi_{\rm L,r} \cos 2\theta_{\rm r} + \Pi_{\rm L,p} \cos 2\theta_{\rm p})/2 \approx 8\%$, where the subscripts refer to the prompt (p) and reverse-shock (r) contributions. The first three observations are dominated by the reverse-shock component and show a low but stable degree of polarization, such that $\Pi_{\rm L,r} \cos 2\theta_{\rm r} \approx 5\%$. By assuming that the reverse-shock polarization remains constant during our last polarimetric exposure, as would be expected in the presence of a large-scale magnetic field[3], we derive $\Pi_{\rm L,p} \cos 2\theta_{\rm p} \approx 11\%$, well below the maximum possible value. Because in general $\theta_{\rm r} \neq \theta_{\rm p}$, the chance that our measurement results from the instrumental set-up is 1% or less. Our data therefore suggest that the distortion of the magnetic-field configuration happens in the early stages of the jet, at a radius comparable to or smaller than the prompt emission radius.

Broadband afterglow modelling. Unless otherwise stated, all the quoted errors are 1σ. The temporal evolution of the X-ray (X), optical (opt) and near-infrared (NIR) afterglow is well described by simple power-law decays ($F \propto t^{-\alpha}$), with slopes $\alpha_{\rm X} = 1.22 \pm 0.06$, $\alpha_{\rm opt} = 0.945 \pm 0.005$ and $\alpha_{\rm NIR} = 0.866 \pm 0.008$ until $T_0 + 14$ days, when the flux is observed to decrease rapidly at all wavelengths with a temporal index $\alpha_{\rm j} = 2.57 \pm 0.04$.

The X-ray spectrum is best fit by an absorbed power-law model with slope $\beta_{\rm X} = 0.92 \pm 0.06$ and only marginal (2σ) evidence for intrinsic absorption, $N_{\rm H,i} = (1.6 \pm 0.8) \times 10^{21}\,\mathrm{cm}^{-2}$, in addition to the galactic value $N_{\rm H} = 9.6 \times 10^{20}\,\mathrm{cm}^{-2}$. A power-law fit performed on the optical/infrared (OIR) data yields negligible intrinsic extinction and a slope of $\beta_{\rm OIR} = 0.50 \pm 0.05$ at $T_0 + 8$ hours, which progressively softens to 0.8 ± 0.2 at $T_0 + 10$ days. The low intrinsic extinction ($E_{\rm B-V}$ is less than 0.06; 95% confidence level) shows that dust scattering has a negligible effect[48] (less than 0.5%) on our measurements of polarization.

Within the external shock model, the difference in temporal and spectral indices indicates that the X-ray and optical/infrared emissions belong to two different synchrotron segments. A comparison with the standard closure relations shows that the observed values are consistent with the regime $\nu_{\rm m} < \nu_{\rm opt} < \nu_{\rm c} < \nu_{\rm X}$ for an electron spectral index of about 2.2. The colour change of the optical/infrared afterglow suggests that the cooling break decreases and progressively approaches the optical range. This feature is distinctive of a forward shock expanding into a medium with a homogeneous density profile[49]. However, the measured radio flux and spectral slope cannot be explained by the same mechanism, and require an additional component of emission, probably powered by a strong reverse shock reheating the fireball ejecta as it propagates backward through the jet. This is also consistent with our observations of a bright optical flash at early times[17]. In order to test this hypothesis, we created seven different spectral energy distributions (SEDs) at different times, ranging from $T_0 + 0.4$ days to $T_0 + 30$ days, and modelled the broadband afterglow and its temporal evolution with a forward shock plus reverse shock (FS + RS) model[17,49]. The best-fit afterglow parameters are an isotropic-equivalent kinetic energy $\log E_{\rm K,iso} = 54.3^{+0.17}_{-0.5}$, a low circumburst density $\log n = -4.0^{+1.7}_{-1.1}$, and microphysical parameters $\log \varepsilon_{\rm e} = -1.0^{+0.5}_{-1.0}$ and $\log \varepsilon_{\rm B} = -2.0 \pm 1.0$. These results are consistent with the trend of a low-density environment and high radiative efficiency observed in other bright bursts[50,51]. Our data and best-fit model are shown in Extended Data Fig. 4.

In this framework, the achromatic temporal break at $T_0 + 14$ days is the result of the outflow geometry, collimated into a conical jet with a narrow opening angle $\theta_{\rm j} = 2.4^{+1.6}_{-0.7}$ deg. This lessens the energy budget by the factor θ_j^2, and the resulting collimation-corrected energy release of about 6×10^{51} erg is within the range of other GRBs. The extreme luminosity of GRB 160625B can therefore be explained, at least in part, by its outflow geometry, as we are viewing the GRB down the core of a very narrow jet.

The large flux ratio between the reverse shock and forward shock at peak, $f_{\rm RS}/f_{\rm FS} > 5 \times 10^3$, implies a high magnetization parameter[52,53] $R_{\rm B} \approx \varepsilon_{\rm B,RS}/\varepsilon_{\rm B,FS} > 100(\Gamma/500)^2 >> 1$, and shows that the magnetic energy density within the fireball is larger than in the forward shock. From our broadband modelling we derived a best-fit value for $\varepsilon_{\rm B,FS}$ of about 0.01, with a 1-dex uncertainty, which allows us to estimate the ejecta magnetic content in the range $\sigma \geq 0.1$, where solutions with σ values greater than 1 would suppress the reverse-shock emission and are therefore disfavoured.

Data availability. All relevant data are available from the corresponding author upon reasonable request. Data presented in Fig. 1 and Extended Data Fig. 1 are included with the paper. Swift XRT data are available at http://www.swift.ac.uk/xrt_products/.

30. Breeveld, A. A. *et al.* An updated ultraviolet calibration for the Swift/UVOT. *Am. Inst. Phys. Conf. Ser.* **1358,** 373–376 (2011).
31. Bertin, E. & Arnouts, S. SExtractor: software for source extraction. *Astron. Astrophys.* **117** (Supp.), 393–404 (1996).
32. Chambers, K. C. *et al.* The Pan-STARRS1 surveys. Preprint available at https://arxiv.org/abs/1612.05560 (2016).
33. Skrutskie, M. F. *et al.* The Two Micron All Sky Survey (2MASS). *Astron. J.* **131,** 1163–1183 (2006).
34. Sault, R. J., Teuben, P. J. & Wright, M. C. H. A retrospective view of MIRIAD. *Astron. Data Analysis Software Systems IV* **77,** 433–436 (1995).
35. Uhm, Z. L. & Zhang, B. Fast-cooling synchrotron radiation in a decaying magnetic field and γ-ray burst emission mechanism. *Nat. Phys.* **10,** 351–356 (2014).
36. Arnaud, K. A. XSPEC: the first ten years. *Astron. Data Analysis Software Systems V* **101,** 17–20 (1996).
37. Band, D. *et al.* BATSE observations of gamma-ray burst spectra. I—spectral diversity. *Astrophys. J.* **413,** 281–292 (1993).
38. Vestrand, W. T. *et al.* A link between prompt optical and prompt γ-ray emission in γ-ray bursts. *Nature* **435,** 178–180 (2005).
39. Shen, R.-F. & Zhang, B. Prompt optical emission and synchrotron self-absorption constraints on emission site of GRBs. *Mon. Not. R. Astron. Soc.* **398,** 1936–1950 (2009).
40. Gendre, B. *et al.* GRB 110205A: anatomy of a long gamma-ray burst. *Astrophys. J.* **748,** 59 (2012).
41. Klotz, A., Boër, M., Atteia, J. L. & Gendre, B. Early optical observations of gamma-ray bursts by the TAROT telescopes: period 2001–2008. *Astron. J.* **137,** 4100–4108 (2009).
42. Kumar, P. & Panaitescu, A. What did we learn from gamma-ray burst 080319B? *Mon. Not. R. Astron. Soc.* **391,** L19–L23 (2008).
43. Yu, Y. W., Wang, X. Y. & Dai, Z. G. Optical and γ-ray emissions from internal forward-reverse shocks: application to GRB 080319B? *Astrophys. J.* **692,** 1662–1668 (2009).
44. Giannios, D. Prompt GRB emission from gradual energy dissipation. *Astron. Astrophys.* **480,** 305–312 (2008).
45. Wei, D. M. The GRB early optical flashes from internal shocks: application to GRB990123, GRB041219a and GRB060111b. *Mon. Not. R. Astron. Soc.* **374,** 525–529 (2007).
46. Li, Z. & Waxman, E. Prompt optical emission from residual collisions in gamma-ray burst outflows. *Astrophys. J.* **674,** L65–L68 (2008).
47. Fan, Y. Z., Zhang, B. & Wei, D. M. Early optical-infrared emission from GRB 041219a: neutron-rich internal shocks and a mildly magnetized external reverse shock. *Astrophys. J.* **628,** L25–L28 (2005).

48. Serkowski, K., Matheson, D. S. & Ford, V. L. Wavelength dependence of interstellar polarisation and ratio of total to selective extinction. *Astrophys. J.* **196,** 261 (1975).
49. Granot, J. & Sari, R. The shape of spectral breaks in gamma-ray burst afterglows. *Astrophys. J.* **568,** 820–829 (2002).
50. Cenko, S. B. *et al.* Afterglow observations of Fermi large area telescope gamma-ray bursts and the emerging class of hyper-energetic events. *Astrophys. J.* **732,** 29 (2011).
51. Ackermann, M. *et al.* Multiwavelength observations of GRB 110731A: GeV emission from onset to afterglow. *Astrophys. J.* **763,** 71 (2013).
52. Zhang, B., Kobayashi, S. & Mészáros, P. Gamma-ray burst early optical afterglows: implications for the initial Lorentz factor and the central engine. *Astrophys. J.* **595,** 950–954 (2003).
53. Zhang, B. & Kobayashi, S. Gamma-ray burst early afterglows: reverse shock emission from an arbitrarily magnetized ejecta. *Astrophys. J.* **628,** 315–334 (2005).

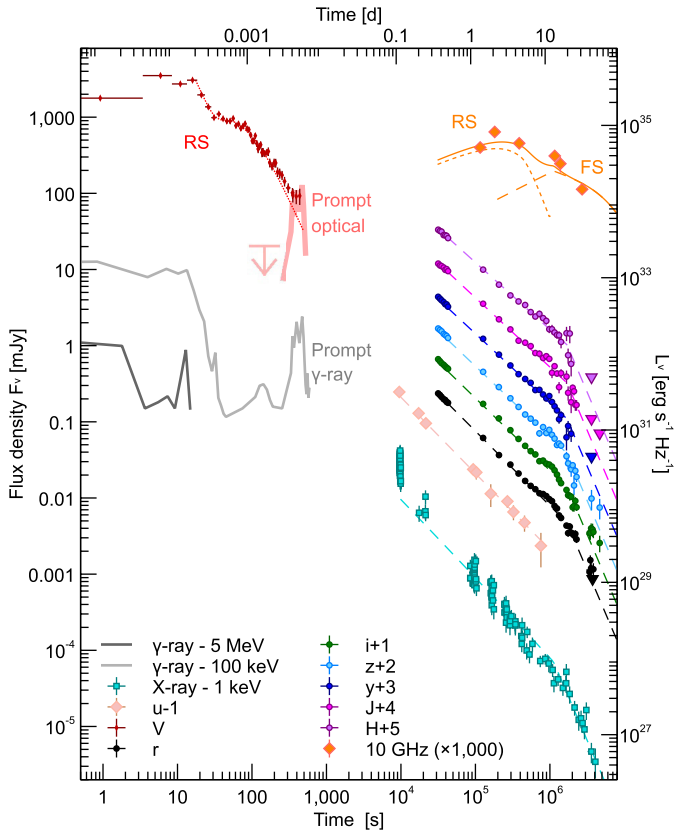

Extended Data Figure 1 | Multiwavelength light curves for GRB 160625B and its afterglow. Different emission components shape the temporal evolution of GRB 160625B. On timescales of seconds to minutes after the explosion, we observe bright prompt (solid lines) and reverse-shock (dotted lines) components. On timescales of hours to weeks after the burst, emission from the forward shock (dashed lines) becomes the dominant component from X-rays down to radio energies. After about 14 days, the afterglow emission falls off at all wavelengths. This phenomenon, known as jet-break, is caused by the beamed geometry of the outflow. Error bars denote 1σ limits; upper limits are 3σ. Times are given with reference to the LAT trigger time T_0. FS, forward shock; RS, reverse shock; a subscript 'ν' refers to frequency; u, V, r, i, z, y, J and H denote specific optical filters.

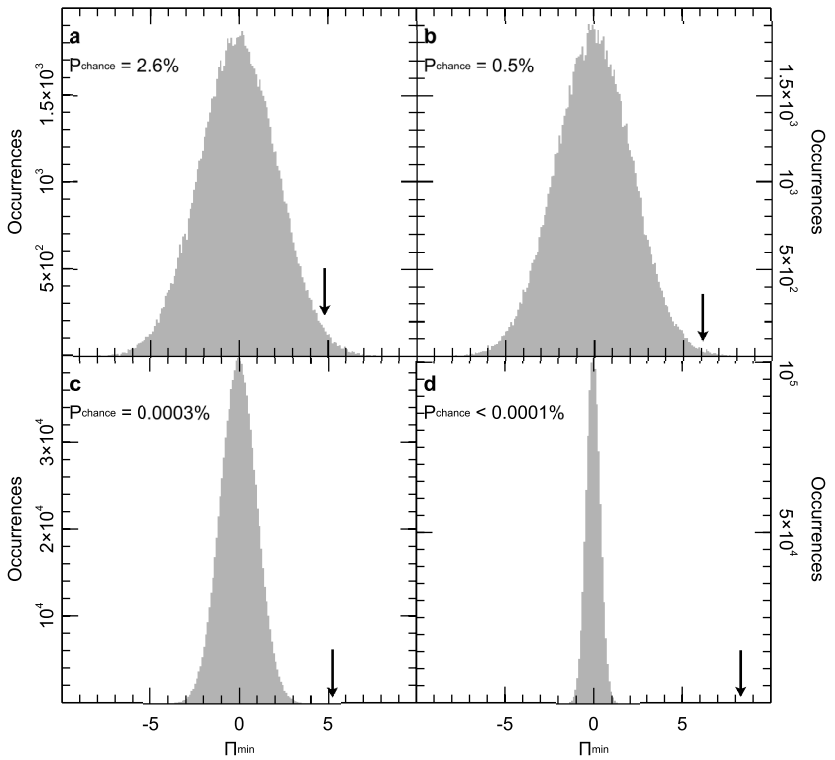

Extended Data Figure 2 | Results of Monte Carlo simulations. For each of the four polarization epochs, we simulated and examined a large number of data sets with similar photometric properties and no intrinsic afterglow polarization. **a**, Results of 10^5 simulations for the first epoch (95–115 seconds). **b**, As for **a**, but for the second epoch (144–174 seconds). **c**, Results of 10^6 simulations for the third epoch (186–226 seconds). **d**, As for **c**, but for the fourth epoch (300–360 seconds). The observed values are shown by vertical arrows. The probability of obtaining by chance a polarization measurement as high as the observed value is also reported. $\Pi_{\rm min}$, minimum polarization value.

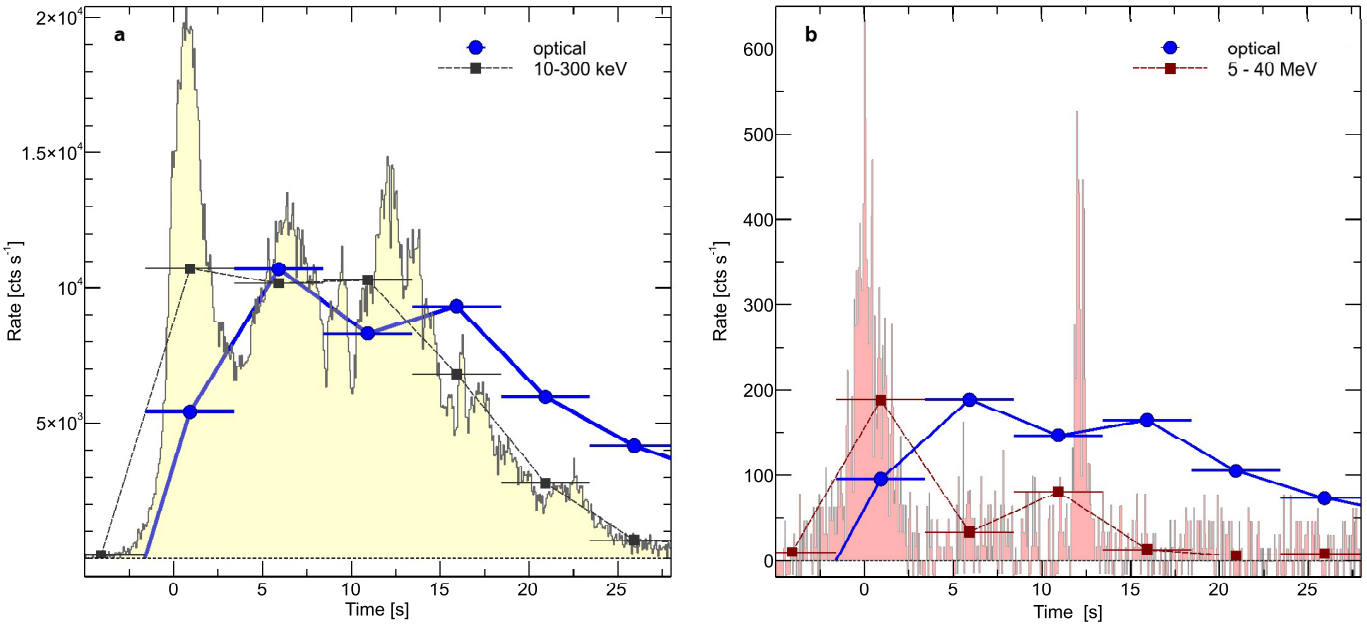

Extended Data Figure 3 | Comparison of the early γ-ray and optical emission measured for GRB 160625B. a, γ-ray light curves in the soft (50–300 keV) energy band. **b**, γ-ray light curves in the hard (5–40 MeV) energy band. Optical data (blue circles) have been arbitrarily rescaled. The squared points (in the background) show the γ-ray light curves re-binned by adopting the same time intervals as for the optical observations. Times are given with reference to the LAT trigger time T_0. The horizontal bars show the time interval (5 s) over which the observation was taken.

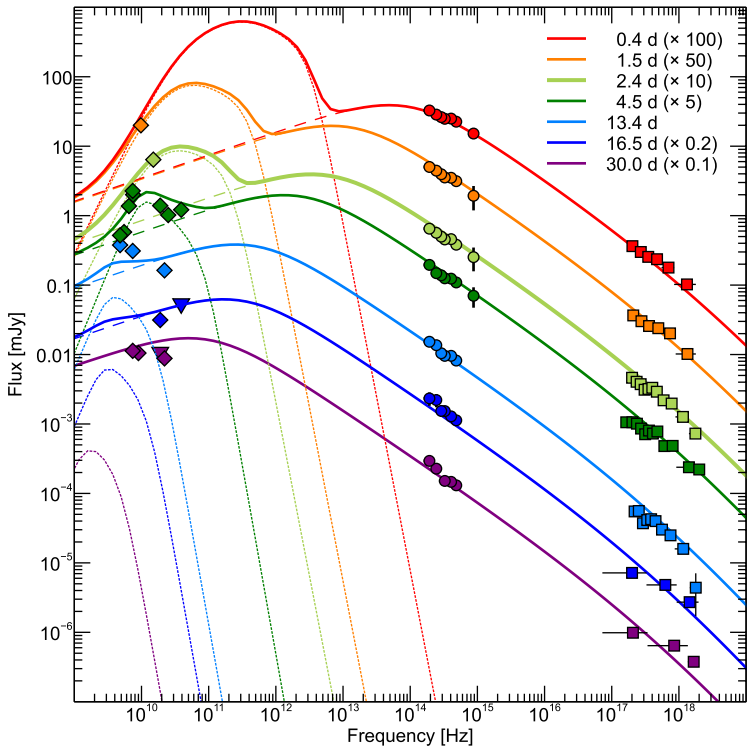

Extended Data Figure 4 | Afterglow spectral energy distributions of GRB 160625B. The afterglow evolution can be described by the combination of forward-shock (dashed lines) and reverse-shock (dotted lines) emission. The best-fit model is shown with solid lines. The peak flux of the forward-shock component is about 0.4 mJy, much lower than the optical flux measured at $T < T_0 + 350$ seconds. This shows that the forward-shock emission is negligible during the prompt phase. Error bars denote 1σ limits; upper limits are 3σ.

Extended Data Table 1 | Polarimetry results

Time since T_0 [mid; s]	Exposure time [s]	$\Pi_{L,min}$ [%]	Error [1 σ; %]
105	20	4.8	1.7
159	30	6.1	1.4
206	40	5.2	0.6
330	60	8.3	0.5

Extended Data Table 2 | Spectral properties of the prompt emission for GRB 160625B

Time interval [s]	Detectors	α	β	E_p [keV]	Flux (10-10^4 keV) [10^{-7} erg cm^{-2} s^{-1}]	W-Stat	dof
0.10-19.10 (G2)	NaI_7, NaI_9, BGO_1	-0.733±0.010	-2.50±0.04	680±20	429±5	250	204
337-607 (G3)	NaI_6, BGO_1	-1.52±0.04	-2.3	140^{+40}_{-30}	2.30±0.10	211	77
Time-Resolved Analysis							
334-359	NaI_6, BGO_1	-1.53±0.02	-2.3	>210	3.2±0.5	60	74
359-384	NaI_6, BGO_1	-1.55±0.03	-2.3	>180	2.4±0.7	58	74
384-414	NaI_6, BGO_1	-1.49±0.02	-2.3	>210	3.9±0.7	67	72
414-464	NaI_6, BGO_1	-1.53±0.04	-2.3	270±80	3.2±0.3	68	73
464-499	NaI_6, BGO_1	-1.45±0.03	-2.3	130±15	4.9±0.3	62	81

The GRB prompt emission can be described by a smoothly broken power law[37] with low-energy index α, high-energy index β, and peak energy E_p. Errors are 1σ; lower limits are at the 95% confidence level. Given the high statistical quality of the G2 spectrum, we added a 5% systematic error to the fit. W-stat is the value of the modified Cash statistic for the best-fit model. dof, degrees of freedom.